Convection Initiation by Density Currents: Role of Convergence, Shear, and Dynamical Organization

MITCHELL W. MONCRIEFF AND CHANGHAI LIU

National Center for Atmospheric Research, Boulder, Colorado*

(Manuscript received 25 February 1998, in final form 8 October 1998)

ABSTRACT

Steady-state analytic models establish two key points concerning the impact of vertical shear on density currents and the implication for convection initiation. First, shear decreases the horizontal convergence, and therefore the mean ascent, associated with downshear propagating currents. Second, shear has a basic effect on the dynamical organization. If the downshear current travels at the speed of the ambient flow at a critical (steering) level, an overturning circulation provides deep lifting. Although mean ascent is increased by shear in the case of upshear propagating currents, the lifting is comparatively shallow because jumplike ascent occurs rather than deep overturning. The convection initiation mechanism involving the downshear current is therefore very different from the upshear case.

These basic principles are borne out in two-dimensional numerical simulations. Density currents generated by a stationary cold source imposed on an initially horizontally homogeneous, sheared, and neutrally stratified ambient flow are explored. Results show that (i) if the surface flow and low-level shear vectors are in the same direction, as in a low-level jet, the effects of shear and surface flow on the density current head height counteract one another; and (ii) if they oppose one another, as in a surface jet, both conspire to lower the density current head on the downwind side but raise it on the upwind side.

As regards convection initiation by sea breezes, point (i) above shows an approximately equal but weak preference for convection exists on the leeward and windward coasts. Point (ii) shows that initiation is strongly suppressed on the windward coast, but strongly enhanced on the leeward one. The hypothesis that sea breezes are more intense in offshore flow therefore holds only if shear and surface flow have opposite sign or if the flow is unsheared.

Concerning convection initiation by thunderstorm outflows, downshear propagating outflows provide the deepest lifting if they move at the speed of the ambient flow at a critical level, despite the fact that low-level convergence is decreased by shear. While shear strengthens the mean ascent in upshear propagating outflows there is no steering level to anchor the incipient convection to the organized ascent.

1. Introduction

The characteristic metastability of the planetary boundary layer means that air has to be lifted through a finite distance before convection is initiated. Density currents are a very effective lifting mechanism and were they less common (i.e., if the boundary layer were typically saturated), the distribution of precipitating convection would almost certainly depart from the observed state. This statement follows from the linear perturbation theory of an unstably stratified shear flow, where the preferred orientation of convection is parallel to the ambient flow, whereas squall lines are commonly aligned perpendicular to the low-level flow. The alignment issue led to the use of localized cooling as a finite-amplitude convection initiation mechanism in numerical models (Moncrieff and Miller 1976) because the orientation of density currents generated by the cooling is consistent with the propensity for squall lines to be flow perpendicular.

A primary example of an atmospheric density current is the outflow of evaporatively cooled downdrafts from thunderstorms (Charba 1974; Goff 1976; Wakimoto 1982; Mueller and Carbone 1987). The interaction of downdraft outflows with ambient shear also affects the life cycle of convection, notably the longevity and dynamical structure of squall lines (Thorpe et al. 1982, hereafter TMM; Rotunno et al. 1988, hereafter RKW). These outflows can trigger convection at great distances from the source if they travel into a favorable environment (Carbone et al. 1990), are subjected to mesoscale oscillations (Crook et al. 1990), or collide with other

* The National Center for Atmospheric Research is sponsored by the National Science Foundation.

Corresponding author address: Dr. Mitchell W. Moncrieff, National Center for Atmospheric Research, P.O. Box 3000, Boulder, CO 80307.
E-mail: moncrief@ucar.edu

outflows and convergence lines (Wilson and Schreiber 1986).

Sea breezes and land breezes are also described by density current dynamics (Simpson 1987). Although horizontal convergence due to differential heating is the ultimate cause of a sea breeze, the horizontal gradient of heating must exceed a critical value before it attains density current characteristics (Reible et al. 1993). Further examples are sharp cold fronts (Clarke 1961; Nielsen and Neilley 1990) and cold-frontal rainbands (James and Browning 1979; Carbone 1982; Hobbs and Persson 1982).

Theoretical and numerical models of density currents are reviewed in Liu and Moncrieff (1996a, hereafter LM96), who focused on the dynamical effects of ambient shear. Density currents in a shear flow have been studied analytically (Moncrieff and So 1989; Xu 1992; Xu and Moncrieff 1994; Liu and Moncrieff 1996b; Xue et al. 1997) and numerically simulated (Chen 1995; Xu et al. 1996).

Although convection initiation by density currents is primarily a function of horizontal convergence, the dynamical role of shear is not fully understood. An issue we emphasize is how shear affects lifting through its dynamical effect on organization. Because we consider unidirectional mean flow, there is little loss of generality in using a two-dimensional framework.

2. Relative effects of surface convergence and shear

The elements of density current dynamics have long been known (von Karman 1940; Benjamin 1968) in terms of the Froude number, which for atmospheric density currents is $F = U_0[g(\Delta\overline{\theta_v}/\overline{\theta_v})h]^{-1/2}$, where h is the far-field depth of the current, U_0 the surface inflow, and $-\Delta\overline{\theta_v}$ the virtual potential temperature deficit in the density current. While the basic dynamics are captured by this classical theory, ambient shear has an influence over and above the bulk effect of the Froude number.

In a motionless environment, density current circulations are symmetric about a vertical plane centered on the cold air source. Uniform flow affects the dynamics through the Froude number. LM96 showed if the ambient flow opposes the system movement (headwind), the density current head is raised compared to calm surroundings while a following wind (tailwind) has the opposite effect.

The horizontal pressure gradient due to the hydrostatic effect of the cold air is basically why a density current propagates. The system-relative flow is strongly affected by the direction of the propagation velocity relative to the shear vector. Because, in our study, the low-level ambient shear is positive, we can unambiguously refer to the density currents as propagating either downshear (the direction of the shear vector) or upshear. LM96 and Xu et al. (1996) showed that weak or moderate shear elevates the head of the downshear-propagating current. When the current propagates at the speed of a sheared ambient flow at a steering level the airflow organization is markedly different. The upshear-propagating density current is steadier and less sensitive to shear than its downshear counterpart and its structure is basically described by classical theory.

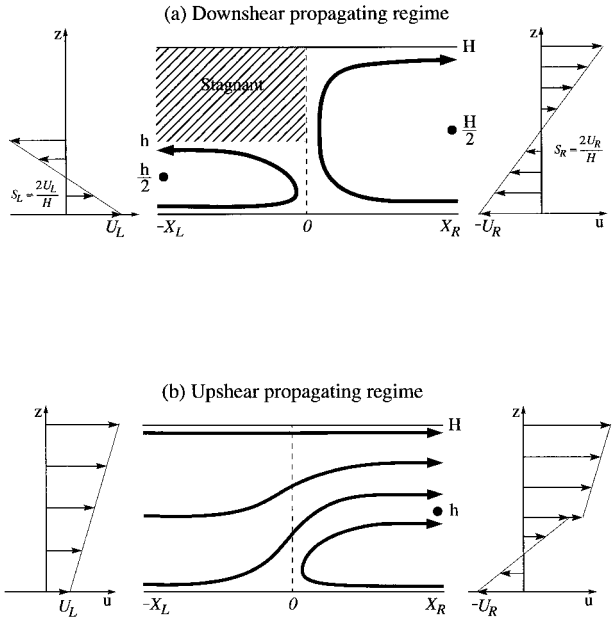

FIG. 1. Schematic of the relative flow in the idealized dynamical model. (a) Downshear-propagating regime and (b) upshear-propagating regime.

a. Downshear propagation

The downshear-propagating model sketched in Fig. 1a has three components: (i) an overturning updraft that moves along with the ambient flow at $z = H/2$, (ii) a density current circulation characterized by a forward-directed surface flow, and (iii) a stagnant layer overlying the density current. Application of the Bernoulli equation to the surface flow relates U_L, U_R and the mean buoyancy in the density current, $-g\Delta\theta/\theta$. Assuming that the remote pressure field is hydrostatic, we obtain

$$\frac{\overline{\Delta\theta}}{\theta} = \frac{1}{2}\frac{U_R^2}{gh}(1 - G_R^2). \tag{1}$$

Because $\Delta\theta$ is nonnegative, $G_R = U_L/U_R \leq 1$ and the strength of the circulation in the cold air inflow is limited by the surface inflow to the density current. If $G_R = 1$, the temperature deficit is zero and the model represents either a gust front or a collision between two currents of equal density in an unstratified environment. Defining the Froude number as $F_R^2 = U_R^2/[g(\Delta\theta/\theta)h]$, we obtain

$$G_R = \sqrt{1 - \frac{2}{F_R^2}}, \tag{2}$$

showing F_R must not be less than $\sqrt{2}$.

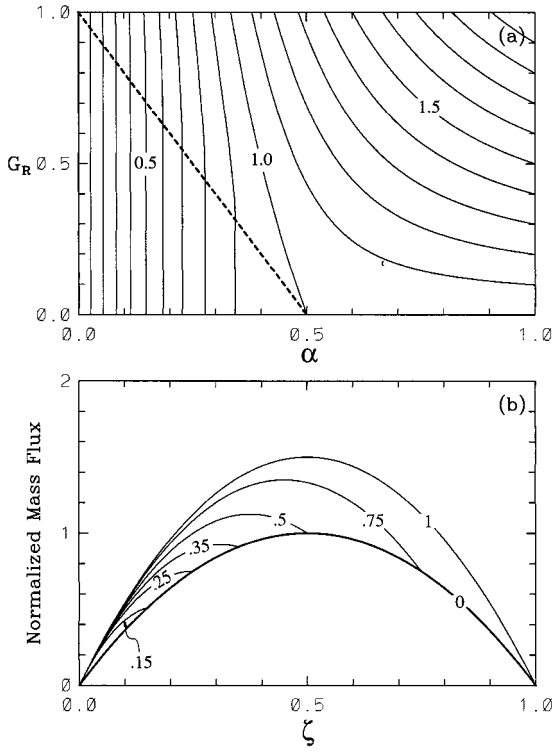

FIG. 2. (a) Isopleths of the normalized average vertical mass flux, $\overline{w}\ (x_R - x_L)/(\frac{1}{4}U_R H)$, in terms of $\alpha = h/H$ and $G_R = U_L/U_R$. (b) Normalized average vertical mass flux as a function of height for $G_R = \frac{1}{2}$ and values of $\alpha = 0$, 0.15, 0.25, 0.35, 0.5, 0.75, and 1.00.

The low-level mean vertical motion caused by the horizontal convergence and the effect of shear on its strength is the key issue in convection initiation. Referring to Fig. 1a and integrating the mass continuity equation in the domain $-x_L \le x \le x_R$; $0 \le z \le H$ gives the mean vertical velocity

$$\overline{w}(z) = \frac{1}{(x_R - x_L)} \int_{x_L}^{x_R} w\, dx, \tag{3}$$

in which case

$$\overline{w}(z)(x_R - x_L) = \begin{cases} (U_R + U_L)z - \frac{1}{2}(S_L + S_R)z^2 & 0 \le z \le h \\ U_R z - \frac{1}{2}S_R z^2 & h \le z \le H, \end{cases} \tag{4}$$

where U_L, U_R, S_L, and S_R are nonnegative. The two terms on the right-hand side of Eq. (4) are the contributions by surface convergence and shear, respectively. Inspection of Eq. (4) shows that shear *decreases* the mean ascent caused by downshear-propagating density currents because horizontal convergence decreases with height.

No vorticity is generated within the overturning updraft; therefore, the height of no relative motion defining the steering level is exactly half the depth of the overturning circulation in which case $U_R = HS_R/2$. For similar reasons $U_L = hS_L/2$. Using Eq. (4) it follows on defining $\zeta = z/H$ and $\alpha = h/H$ that the ratio of the horizontally averaged updraft mass flux to the total inflow mass flux is

$$\frac{\overline{w}(x_R - x_L)}{\frac{1}{4}U_R H} = \begin{cases} 4\alpha\left[(1 + G_R)\dfrac{\zeta}{\alpha} - (\alpha + G_R)\left(\dfrac{\zeta}{\alpha}\right)^2\right] & 0 \le \zeta \le \alpha \\ 4\zeta(1 - \zeta^2) & \alpha \le \zeta \le 1. \end{cases} \tag{5}$$

The mean vertical motion is a maximum at $z_m = (U_R + U_L)/(S_L + S_R)$; that is, $\zeta_m/\alpha = (1 + G_R)/2(\alpha + G_R)$. The left-hand side of Eq. (5) represents the total vertical mass flux normalized by the averaged inflow mass flux. Figure 2a shows the solution of Eq. (5) for $\zeta = \zeta_m$ ($z = z_m$). The dashed line denotes the special case $\zeta_m = \alpha$ ($z_m = h$) and divides the solution domain into two parts. The region on the right-hand side corresponds to $\zeta_m \le \alpha$ ($z_m \le h$), whereas that on the left corresponds to $\zeta_m > \alpha$. In the latter, the maximum mass flux is obtained by setting $\zeta = \alpha$ instead of $\zeta = \zeta_m$. The results indicate that while the maximum mass flux is proportional to the cold pool depth, it is insensitive to the variation of G_R, provided the cold pool is shallow.

Figure 2b presents the profiles of the mass transports for $G_R = \frac{1}{2}$. Note that the solution for $\zeta > \alpha$ ($z > h$) is, in any case, the same as in the absence of a cold pool (i.e., $\alpha = 0$). Three kinds of distribution occur corresponding to a single maximum at $\zeta = \frac{1}{2}$ when $\alpha < \frac{1}{4}$, dual maxima at $\zeta = \zeta_m$ and $\zeta = \frac{1}{2}$ when $\frac{1}{4} < \zeta < \frac{1}{2}$, and a single maximum at $\zeta = \zeta_m$ when $\zeta > \frac{1}{2}$, respectively.

If R is the ratio of the shear term and the horizontal convergence term in Eq. (4), it follows that

$$R = \frac{(S_L + S_R)z}{HS_R + hS_L} \tag{6}$$

for $0 \le z \le h$. Note that R vanishes at $z = 0$ where the horizontal convergence is a maximum.

Integrating from $z = 0$ to an arbitary height gives the average effect of shear on average ascent,

$$\overline{S} = \frac{1}{6}(S_L + S_R)z^2, \tag{7}$$

and the average effect of horizontal convergence on average ascent,

$$\overline{C} = \frac{1}{2}(U_L + U_R)z. \tag{8}$$

Defining the $\beta = S_L/S_R$, it follows that

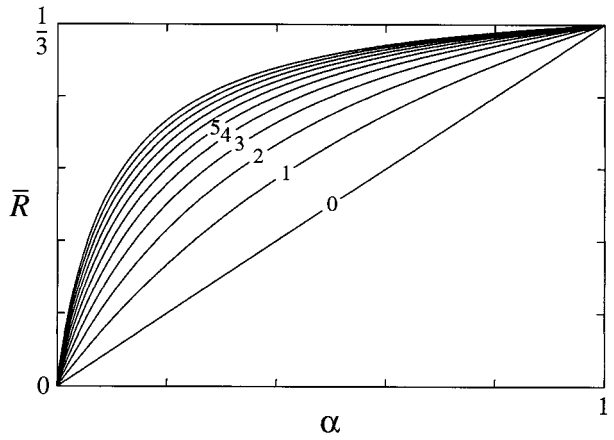

FIG. 3. Relationship between the ratio of shear and convergence effects on mean ascent ($\overline{R}$) against the normalized density current height (α) in isopleths of the ratio of shear in the density current and the environment (β). These curves are solutions of Eq. (9) for $\zeta = \alpha/2$.

$$\overline{R} = \frac{\overline{S}}{\overline{C}} = \frac{2(1 + \beta)\zeta}{3(1 + G_R)}. \tag{9}$$

Figure 3 shows the solution of Eq. (9) in terms of the variation of $\overline{R}$ with α expressed in isopleths of β. The case of $\zeta = \alpha/2$ corresponds to the midlevel of the density current. The maximum value $\overline{R}_{\max} = ⅓$ occurs when the mean vertical motion is a maximum.

In summary, while shear decreases the horizontal convergence due to the downshear-propagating gravity current, it is nevertheless fundamental to the dynamical organization. In particular, the overturning branch lifts boundary layer air to much higher levels than the density current head alone can achieve.

b. Upshear propagation

The flow relative to the upshear propagating density current is shown in Fig. 1b. A kinetic energy discontinuity $\Delta[\frac{1}{2}u^2]$ occurs at $z = h$. This value is obtained by applying the Bernoulli equation along the lower boundary and the two streamlines on either side of the density current interface to give

$$\Delta\left[\frac{1}{2}u^2\right] = \frac{U_R^2}{F_R^2}, \tag{10}$$

where $\Delta[\ ]$ is the difference operator. The interface separating the jump updraft from the density current is a vortex sheet (which may or may not be dynamically stable).

It can be shown that in this case

$$\overline{w}(z)(x_R - x_L) = (U_R + U_L)z + \frac{1}{2}(S_L - S_R)z^2 \tag{11}$$

for $0 \le z \le h$. The effect of shear on convergence depends on the sign of $(S_L - S_R)$. In contrast to the downshear regime, shear can *increase* the horizontal convergence and mean ascent in the upshear-propagating density current. For the special case $S_R = S_L$, Eq. (11) shows mean ascent increases linearly with height. However, no overturning branch exists to accentuate lifting—further evidence of shear-induced dynamical organization.

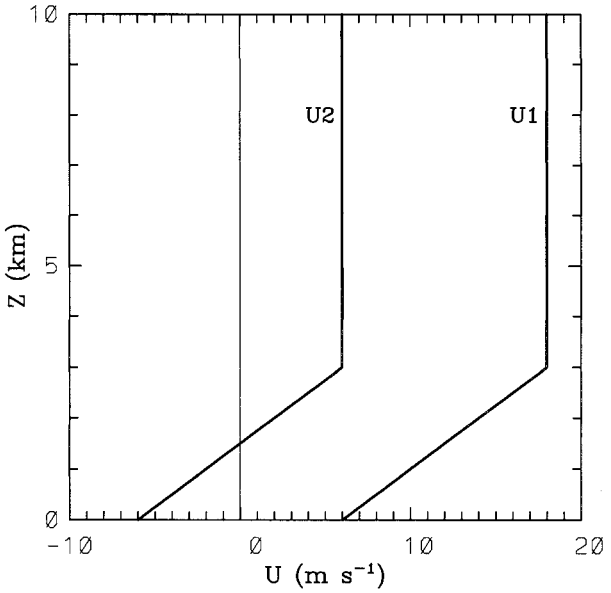

FIG. 4. Ambient flow relative to the cold source used to initialize the numerical simulations.

3. Numerical simulations

Consider a time-invariant, earth-stationary temperature perturbation in a column of height d and width l. The maximum temperature deficit is $\Delta\theta = -8$ K at the lower boundary, decreasing linearly to zero at $z = d$. Scaling length, velocity, and pressure by l, U_s, and the averaged quantity DCAPE $= g(\overline{\Delta\theta}/\theta)d$ defines the *convective* Froude number (or inverse Richardson number) for the cold pool $F_d = U_s(\text{DCAPE})^{-1/2}$. This is a simple way to relate our results to evaporative cooling in downdrafts.

Since the ambient flow profile is uniquely determined by the surface flow and the shear, the shear flow relative to the cold source is

$$U_0(z) = \begin{cases} U_s + Sz & 0 \le z \le h_s \\ U_s + Sh_s & h_s < z \le H, \end{cases} \tag{12}$$

where S is the shear; h_s and H are the depth of the shear layer and that of the model, respectively; and U_s is the surface wind speed. The two profiles used are plotted in Fig. 4.

We conducted a pair of two-dimensional numerical simulations using a dry version of the Clark et al. (1996) numerical model, initialized with a horizontally homogeneous wind profile and a uniform potential tem-

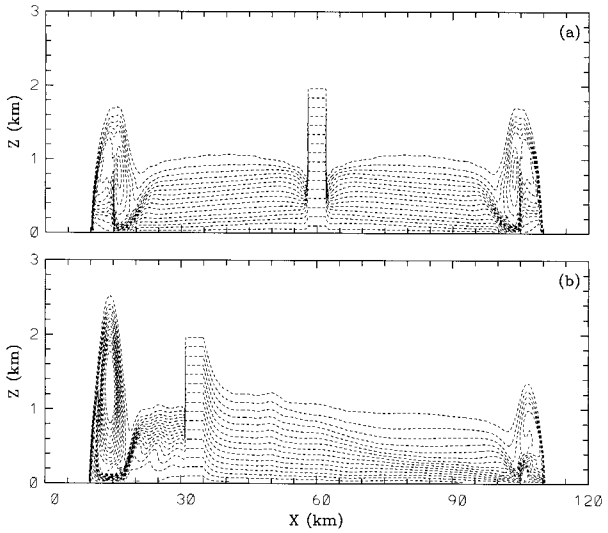

FIG. 5. Potential temperature perturbation after 1 h of simulation for (a) a motionless base state, and (b) unsheared ambient flow of 10 m s^{-1}. Contours start at -0.1 K with interval of 0.5 K (from LM96).

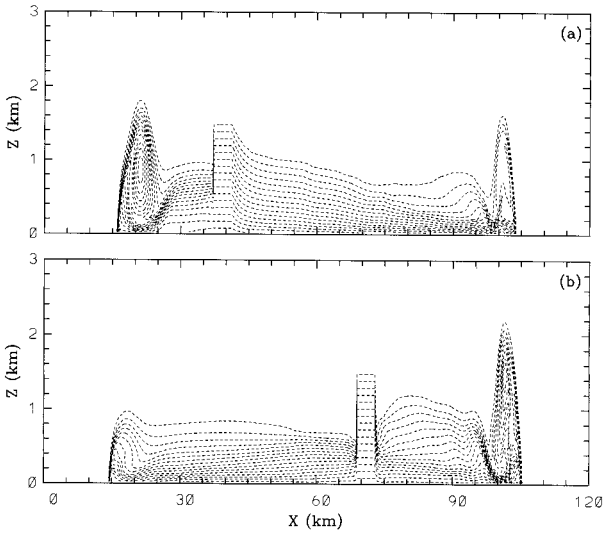

FIG. 6. Potential temperature perturbation after 1 h of simulation for wind profiles (a) U1 and (b) U2. Contours start with -0.1 K, and interval is 0.5 K.

perature of $\theta_0 = 300$ K. For simplicity we considered a fully mixed (neutrally stratified) planetary boundary layer. The two-dimensional domain is 160 km $\times$ 10 km. Constant 100-m grid intervals are used in both vertical and horizontal directions. As shown in Fig. 4, we set $h_s = 3$ km, $d = 2$ km, $l = 4$ km, and $S = 4$ m s^{-1} km^{-1}. We assume S is a positive constant, so the combined effect of shear and surface flow is measured by $U_s = \pm 6$ m s^{-1}. Note that LM96 examined the impact of varying h_s and S (see their Fig. 13).

Density currents propagate rightward and leftward from the buoyancy source. Although the same shear affects both, the flows relative to the left-moving and right-moving currents are very different. LM96 showed how the ambient shear and the surface velocity affect the height of the density current head. Referring to the left-moving current in Fig. 5b, a headwind (ambient flow in the opposite direction to the direction of travel of the density current, which is synonomous to upstream movement) raises the head height compared to calm surroundings in Fig. 5a. On the other hand, examination of the right-moving current in Fig. 5b shows that a tailwind lowers the head height.

When the shear and surface flow vectors are in the same direction (experiment U1), the potential temperature perturbation (Fig. 6a) and the vertical velocity (Fig. 7a) show that the upshear current is deeper and stronger. This behavior is broadly consistent with the Froude number effect of a constant ambient flow (Fig. 5). However, when the shear and surface wind oppose each other (experiment U2), the opposite response occurs: the downshear current is deeper and more intense than its upshear counterpart (Figs. 6b and 7b). This is due to the combined effect of convergence (cf. Figs. 5a and 5b) and shear (cf. Fig. 4 and Fig. 9a of LM96) on density current dynamics.

The flow relative to the upshear and downshear head of U1 is shown in Figs. 8a and 8b, where the propagation speeds are approximately 6 and 17 m s^{-1}, respectively. The corresponding relative flows for U2 are shown in Figs. 8c and 8d, where the propagation speeds are 15 and 9.5 m s^{-1}, respectively. Figure 9 shows that the most obvious difference in the maximum vertical velocity between the upshear and downshear currents occurs for the U2 profile; the relative flows in the upstream and downstream currents are very different (section 4).

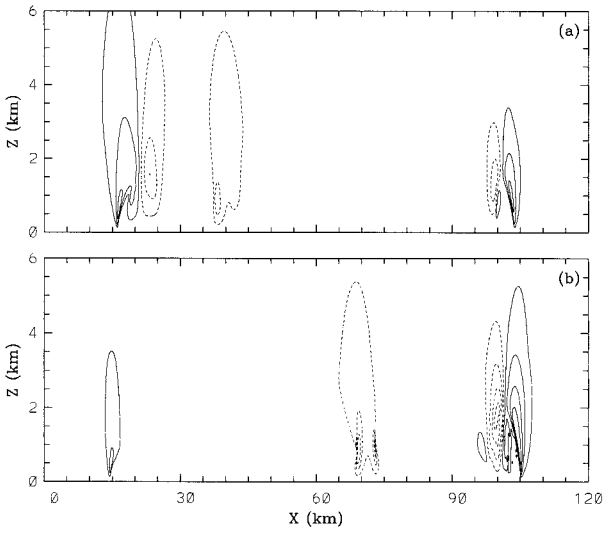

FIG. 7. As in Fig. 6 but for the vertical velocity. The first continuous line and dashed line correspond to 1 m s^{-1} and -1 m s^{-1}, respectively. Contour interval is 2 m s^{-1}.

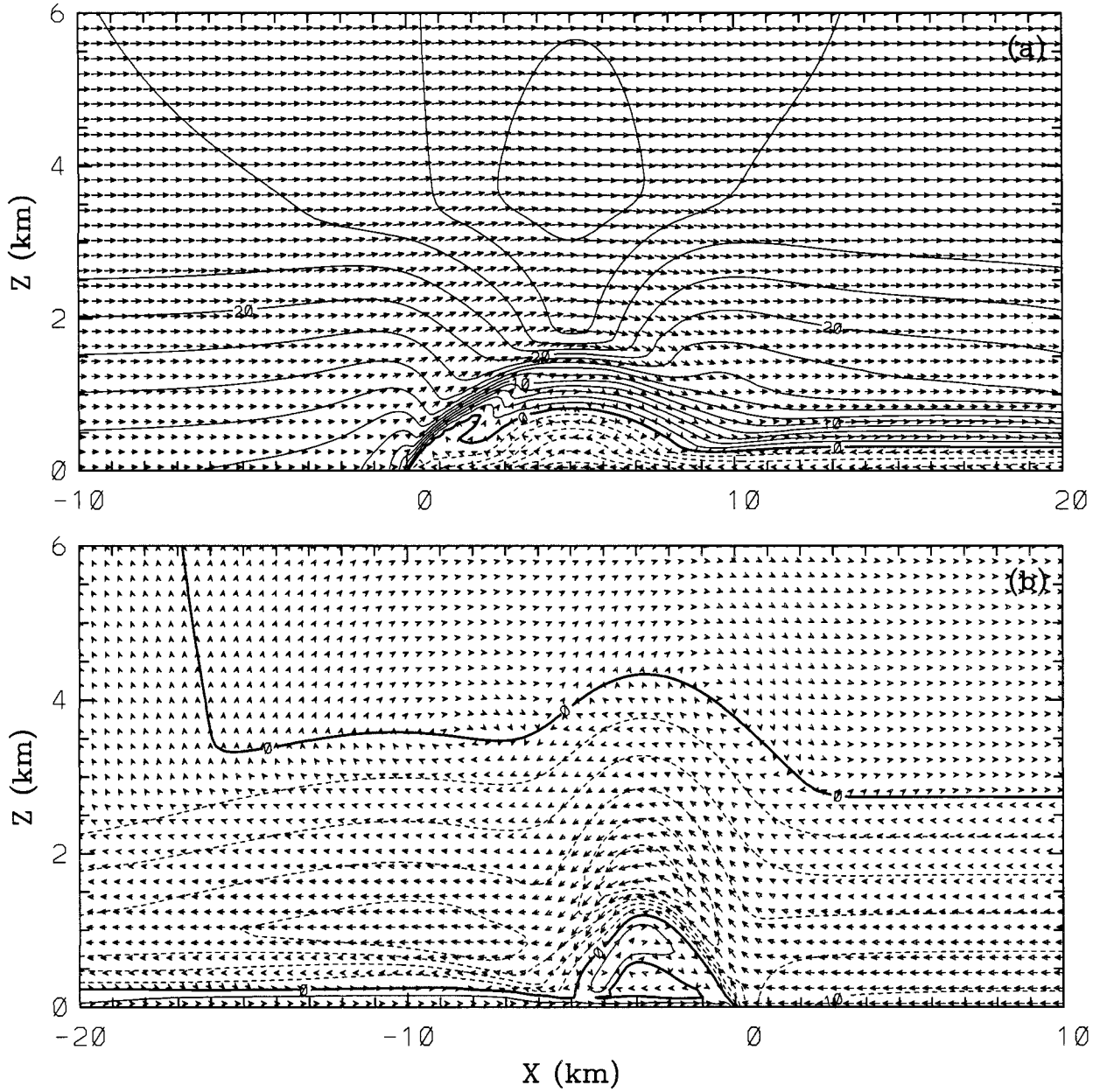

FIG. 8. System-relative horizontal flow and vector field after 1 h of simulation. (a) Upshear-propagating density current for U1; (b) downshear current for U1; (c) upshear current for U2; and (d) downshear current for U2. The contour interval is 2 m s^{-1}.

We examined two-dimensional density currents. Because the cross-stream effects of unidirectional ambient flow on three-dimensional density currents are second order, useful inferences can be made without invoking three-dimensional simulations. For instance, Fig. 5 approximates the transverse dynamical structure and Fig. 6 the streamwise structure.

4. Convection initiation

By definition convection will be initiated if air is lifted to the level of free convection (LFC). The strongest lifting occurs in organized flow of the type sketched in Fig. 1a, which is realized in Figs. 11b and 17b of LM96 and Fig. 8b herein.

a. Sea-breeze fronts

Because the cool air travels outward in opposite directions from the source region, the initial conditions for numerical simulations are more closely identified with a land breeze than with a sea breeze. However, provided we focus on the mature state, our simulations can be interpreted in terms of sea-breeze fronts. The

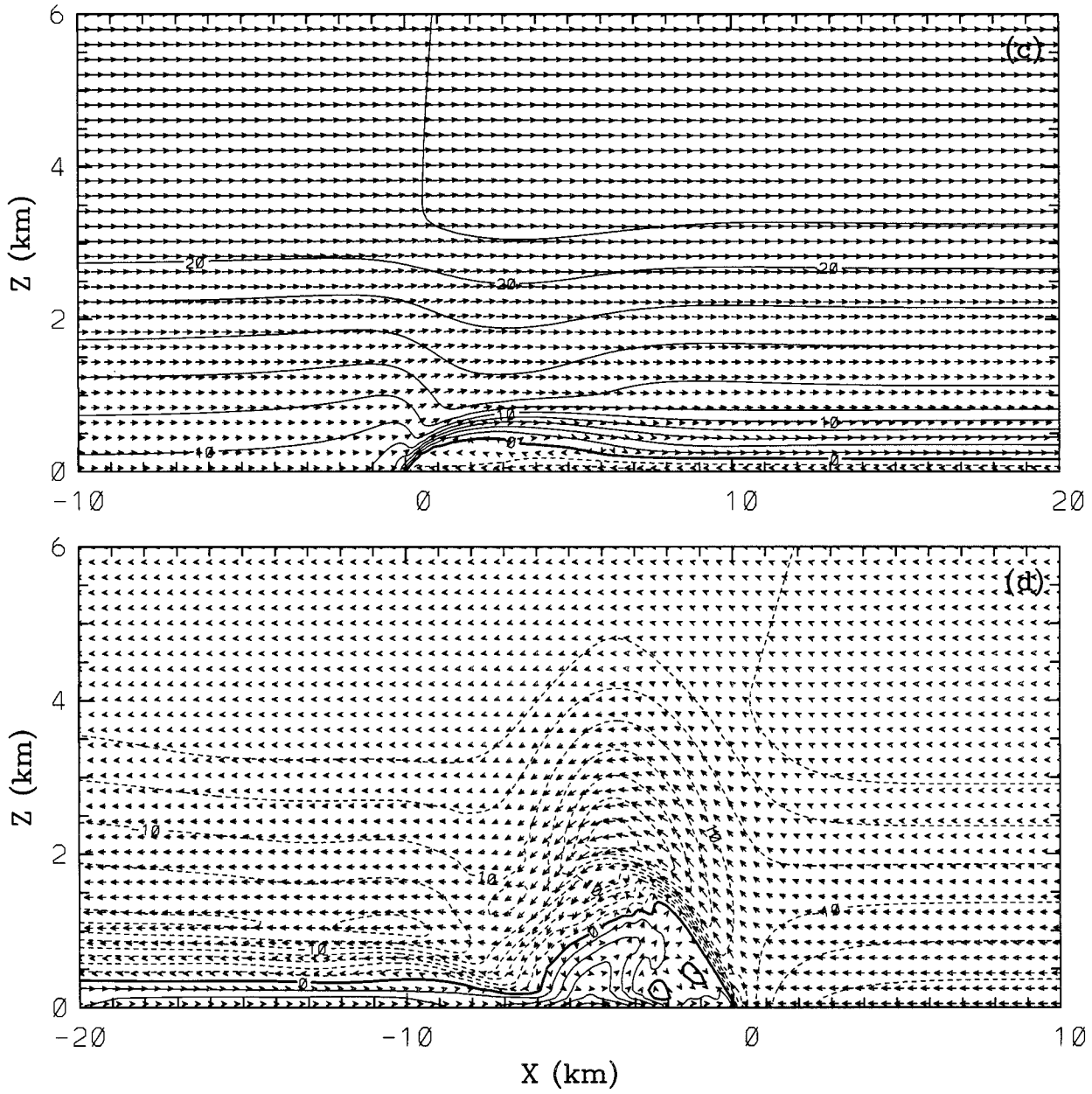

FIG. 8. *(Continued)*

dependence of the sea breeze on the direction of the mean flow has long been known (Wexler 1946) but only recently quantified through aircraft and remote sensing measurements. In particular, the observational studies of sea-breeze events during the Maritime Continent Thunderstorm Experiment (MCTEX; Keenan et al. 1997) and the Convection Initiation and Precipitation Experiment (Atkins and Wakimoto 1997) showed that offshore flows correspond to stronger sea-breeze frontogenesis and are more favorable for thunderstorm initiation than onshore flows.

Shear has received little attention in sea-breeze dynamics. Our results show how the wind (shear) profile affects convection initiation over low-lying islands and peninsulas by the downshear-propagating regime. For wind profiles in which the surface flow and the low-level shear vector point in the same direction, as in the jetlike profile in Fig. 10a, the effects of surface wind and shear counteract each other on *both leeward and windward* coasts. In other words, their combined effect is smaller than either acting alone. For the wind profile in Fig. 10b, the surface flow and shear have opposite sign. Because shear and surface wind both act to depress the density current head on the windward coast, the

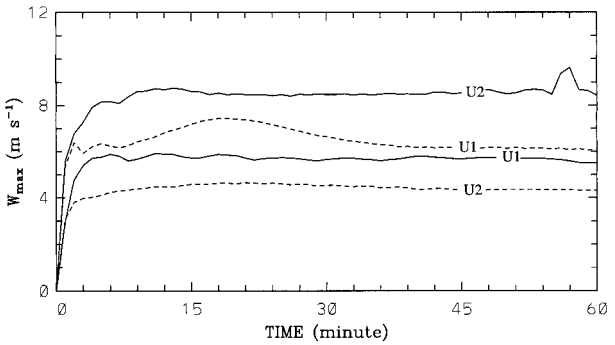

FIG. 9. Evolution of the maximum vertical velocity for the downshear-propagating density current (solid) and upshear current (dashed).

potential for convection initiation is small. Conversely, the mutual reinforcement on the leeward coast (offshore flow) defines it as the preferred location for convection. It follows that in offshore flow sea breezes are stronger *only if* the low-level shear vector and the surface flow are in opposing directions.

During the onset of the Australian monsoon, the lower-tropospheric easterly winds over the Melville and Bathurst (Tiwi) Islands, the site of MCTEX, change from an easterly to a westerly direction (cf. the profiles in Figs. 10a and 10b). Because the major axis of the Tiwi Islands is parallel to the low-level winds, sea breezes commonly originate at the north and south coasts. This means they are not greatly influenced by the mean flow, so the motionless base-state simulation in Fig. 2a is a reasonable approximation. However, during the MCTEX Intensive Observation Period on 4 December 1995, convection started on the lee coast of the Tiwi Islands, when the surface winds were westerly and the low-level shear easterly; an observation consistent with our findings.

In MCTEX, convection initiation is complicated by the interaction between sea-breeze fronts and density currents generated by evaporatively cooled downdraft outflows from preexisting storms that are important in convection initiation (see section 4b). While the temperature deficits in downdrafts are usually larger than in sea breezes, lifting is not determined by thermodynamic considerations alone. Rather, it is a function of the Froude number, the existence of a steering level in the wind profile and the thermodynamic state of the planetary boundary layer measured in terms of the LFC. Measurements made in MCTEX, together with accompanying numerical modeling, are an opportunity to evaluate our findings in terms of both sea breezes and thunderstorm outflow. In this regard Crook (1997) simulated the life cycle of thunderstorm complexes initiated by cold pools from storms that were, in turn, initiated by sea-breeze circulations.

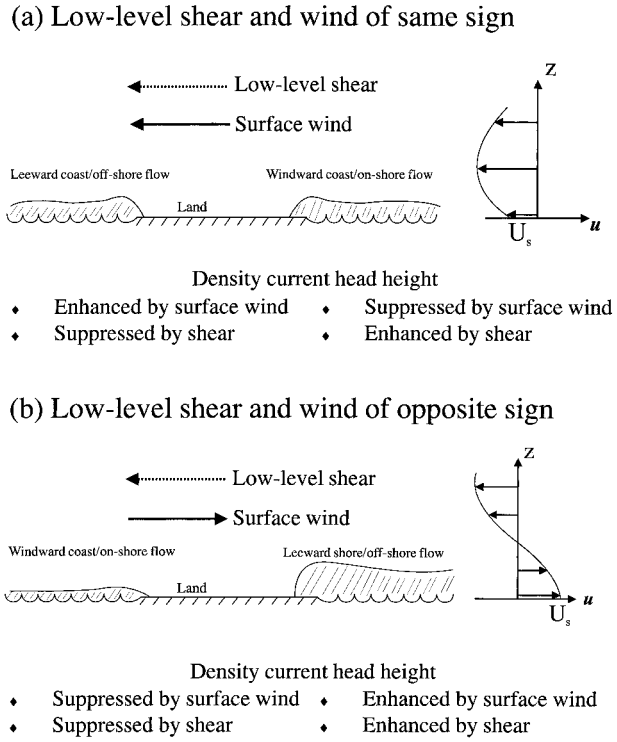

FIG. 10. Schematic diagram of the response of sea breezes to low-level shear and surface flow in (a) same direction and (b) opposite direction.

b. Thunderstorm outflows (cold pools)

A direct application of our results is to density currents generated by evaporatively cooled downdrafts. The form of wind profile in Fig. 4 in which shear is concentrated in low levels has often been used in squall line simulations, notably TMM and RKW. There are several hypotheses on the role of the low-level shear and its interaction with the cold pool, especially for downshear propagation. TMM emphasized the role of low-level convergence. Lafore and Moncrieff (1989) argued that the primary role of shear is its overall or ''global'' effect on flow organization. RKW theorized an optimal state in which the inflow shear is balanced by the vorticity in the cold pool with the optimal flow being a vertically directed jet. The overturning updraft is such a jet and the model in Fig. 1a shows how it is an integral part of the global dynamics. Note that the particular case of $h = H$ and $U_L = U_R$ in Fig. 1a is an example of an optimal state. The RKW theory has often been quoted ipse dixit as implying that low-level shear necessarily benefits deep lifting and convection initiation. Our dynamical arguments show this attribution is incomplete because low-level shear actually *decreases* the mean ascent. The overarching point is that shear affects the upshear and downshear regimes in fundamentally different ways (cf. Figs. 1a and 1b). Dynamical organization is therefore the key aspect, especially the

overturning updraft in density current systems that have a steering level (i.e., the downshear propagating ones).

Depending on the height of the LFC, either upshear- or downshear-propagating density currents could initate convection. Initiation by the shallow lifting in the upshear case requires a low LFC, whereas the deep lifting associated with the overturning updraft could initiate convection even with a high LFC. If the downshear regime has a steering level, the incipient convection cells will remain stationary relative to the organized lifting (Figs. 1a, 8b, and 8d). In the upshear case, on the other hand, even if convection occurs, it will be swept rapidly rearward by the strong relative flow over the density current (Figs. 1b, 8a, and 8c). In other words, while shear may cause stronger mean ascent, there is no deep overturning updraft to accentuate lifting and anchor incipient convection to the organized lifting.

5. Conclusions

It may be a surprise that basic issues remain in density current dynamics and convection initiation in view of the copious literature on these subjects but then the effects of shear on density currents have been little studied. We used analytic models and numerical realizations to put the relative roles of horizontal convergence, shear, and dynamical organization into perspective. Ambient shear reduces the mean ascent in the downshear-propagating case and affects the dynamical organization in a fundamental way. The organizing role of shear is therefore paramount.

Regarding the downshear-propagating regime and convection initiation over peninsulas/islands, (i) when of the same sign, low-level shear and the surface wind (Fig. 10a) are counteractive on both leeward and windward coasts. (ii) When of opposite sign, as in Fig. 10b, the dynamic lifting is a minimum on the windward coast and a maximum on the leeward one. Thus the widely held opinion that sea breezes are more intense in offshore flow holds only if shear and surface flow are in the opposite direction or if the low-level flow is unsheared.

Dynamical organization is also a key issue in convection initiation by downdraft outflows. In downshear-propagating outflows, although shear decreases the mean ascent, the overturning updraft provides deep lifting. This kind of updraft requires that the density current propagates at the speed of the ambient flow at a critical (steering) level. Equation (4) shows the mean ascent in unsheared flow is larger by $\frac{1}{2}S_R z^2$ (e.g., by 4 m s^{-1} at 1 km for the profile in Fig. 4) than in ambient flow of shear S_R. However, unsheared inflow is associated with a front-to-rear (jump) updraft, similar to that in the upshear-propagating current, which is not conducive to deep lifting. Density currents in unsheared flow and upstream-propagating currents in a sheared flow therefore have a similar potential for convection initiation.

Finally, Moncrieff (1989) drew attention to the stagnant (degenerate overturning circulation) overlying the inflow to narrow cold-frontal rainbands, which are intermediate between squall lines and density currents in terms of intensity. The effect of shear on narrow cold-frontal rainbands should be investigated in order to evaluate our findings in terms of a broad class of organized small-scale structures in a sheared flow.

Acknowledgments. MWM acknowledges Greg Holland and Tom Keenan, BMRC, Melbourne, Australia, for the opportunity to be involved in MCTEX, which largely motivated this study. We are grateful to Conrad Ziegler and to the anonymous reviewers for their helpful suggestions.

REFERENCES

Atkins, N. T., and R. M. Wakimoto, 1997: Influence of the synoptic-scale flow on sea breezes observed during CaPE. *Mon. Wea. Rev.,* **125,** 2112–2130.

Benjamin, T. B., 1968: Gravity currents and related phenomena. *J. Fluid Mech.,* **31,** 209–248.

Carbone, R. E., 1982: A severe frontal rainband. Part I: Stormwide hydrodynamic structure. *J. Atmos. Sci.,* **39,** 258–279.

——, J. W. Conway, N. A. Crook, and M. W. Moncrieff, 1990: The generation and propagation of a nocturnal squall line. Part I: Observations and implications for mesoscale predictability. *Mon. Wea. Rev.,* **118,** 25–49.

Charba, J., 1974: Application of gravity current model to analysis of squall-line gust front. *Mon. Wea. Rev.,* **102,** 140–156.

Chen, C., 1995: Numerical simulations of gravity currents in uniform shear flows. *Mon. Wea. Rev.,* **123,** 3240–3253.

Clark, T. L., W. D. Hall, and J. L. Coen, 1996: Source code documentation for the Clark–Hall cloud-scale model: Code Version G3CH01. NCAR Tech. Note. NCAR/TN-426+STR.

Clarke, R. H., 1961: Mesostructure of dry cold fronts over featureless terrain. *J. Meteor.,* **18,** 715–735.

Crook, N. A., 1997: Simulation of convective storms over the Tiwi Islands and comparison with observations from MCTEX. BMRC Research Rep. 64, 7–10.

——, R. E. Carbone, M. W. Moncrieff, and J. W. Conway, 1990: The generation and propagation of a nocturnal squall line. Part II: Numerical simulations. *Mon. Wea. Rev.,* **118,** 50–65.

Goff, R. C., 1976: Vertical structure of thunderstorm outflows. *Mon. Wea. Rev.,* **104,** 1429–1440.

Hobbs, P. V., and P. O. G. Persson, 1982: The mesoscale and microscale structure and organization of clouds and precipitation in midlatitude cyclones. Part V: The substructure of narrow cold-frontal rainbands. *J. Atmos. Sci.,* **39,** 280–295.

James, P. K., and K. A. Browning, 1979: Mesoscale structure of line convection at surface cold fronts. *Quart. J. Roy. Meteor. Soc.,* **105,** 371–382.

Keenan, T., K. Saito, R. E. Carbone, and J. W. Wilson, 1997: The Maritime Continent Thunderstorm Experiment (MCTEX): Observed lifecycle and some initial model simulations. BMRC Research Rep. 64, 3–5.

Lafore, J.-P., and M. W. Moncrieff, 1989: A numerical investigation of the organization and interaction of the convective and stratiform regions of tropical squall lines. *J. Atmos. Sci.,* **46,** 521–544.

Liu, C., and M. W. Moncrieff, 1996a: A numerical study of the effects of ambient flow and shear on density currents. *Mon. Wea. Rev.,* **124,** 2282–2303.

——, and ——, 1996b: An analytical study of density currents in sheared, stratified fluids including the effects of latent heat release. *J. Atmos. Sci.,* **53,** 3303–3312.

Moncrieff, M. W., 1989: Analytic models of narrow cold-frontal rainbands and related phenomena. *J. Atmos. Sci.,* **46,** 150–162.

——, and M. J. Miller, 1976: The dynamics and simulation of tropical cumulonimbus and squall lines. *Quart. J. Roy. Meteor. Soc.,* **102,** 373–394.

——, and D. W. K. So, 1989: A hydrodynamical theory of conservative bounded density currents. *J. Fluid. Mech.,* **198,** 177–197.

Mueller, C. K., and R. E. Carbone, 1987: Dynamics of a thunderstorm outflow. *J. Atmos. Sci.,* **44,** 1879–1898.

Nielsen, J. W., and P. P. Neilley, 1990: The vertical structure of New England coastal fronts. *Mon. Wea. Rev.,* **118,** 1793–1807.

Reible, D. D., J. E. Simpson, and P. F. Linden, 1993: The sea breeze and gravity-current frontogenesis. *Quart. J. Roy. Meteor. Soc.,* **119,** 1–16.

Rotunno, R., J. B. Klemp, and M. L. Weisman, 1988: A theory for strong, long-lived squall lines. *J. Atmos. Sci.,* **45,** 463–485.

Simpson, J. E., 1987: *Gravity Currents in the Environment and Laboratory.* Ellis Horwood Limited, 244 pp.

Thorpe, A. J., M. J. Miller, and M. W. Moncrieff, 1982: Two-dimensional lines. *Quart. J. Roy. Meteor. Soc.,* **108,** 739–761.

von Karman, T., 1940: The engineer grapples with non-linear problems. *Bull. Amer. Math. Soc.,* **46,** 615–683.

Wakimoto, R. M., 1982: The life cycle of thunderstorm gust fronts as viewed with Doppler radar and rawisonde data. *Mon. Wea. Rev.,* **110,** 1060–1082.

Wexler, R., 1946: Theory and observations of land and sea breezes. *Bull. Amer. Meteor. Soc.,* **27,** 272–287.

Wilson, J. W., and W. E. Schreiber, 1986: Initiation of convective storms at radar-observed boundary-layer convergence lines. *Mon. Wea. Rev.,* **114,** 2516–2536.

Xu, Q., 1992: Density currents in shear flows: A two-fluid model. *J. Atmos. Sci.,* **49,** 511–524.

——, and M. W. Moncrieff, 1994: Density current circulations in shear flows. *J. Atmos. Sci.,* **51,** 434–446.

——, M. Xue, and K. E. Droegemeier, 1996: Numerical simulations of density currents in sheared environments within a vertically confined channel. *J. Atmos. Sci.,* **53,** 770–786.

Xue, M., Q. Xu, and K. E. Droegemeier, 1997: A theoretial and numerical study of density currents in nonconstant shear flows. *J. Atmos. Sci.,* **54,** 1998–2019.